Memory-based Ensemble Learning in CMR Semantic Segmentation

Yiwei Liu[1,2], Ziyi Wu[1,2], Liang Zhong[2], Linyi Wen[1,3], Yuankai Wu[1]

[1] Sichuan University
[2] National University of Singapore
[3] West China Women's and Children's Hospital

Abstract. Existing models typically segment either the entire 3D frame or 2D slices independently to derive clinical functional metrics from ventricular segmentation in cardiac cine sequences. While performing well overall, they struggle at the end slices. To address this, we leverage spatial continuity to extract global uncertainty from segmentation variance and use it as memory in our ensemble learning method, Streaming, for classifier weighting, balancing overall and end-slice performance. Additionally, we introduce the End Coefficient (EC) to quantify end-slice accuracy. Experiments on ACDC and M&Ms datasets show that our framework achieves near-state-of-the-art Dice Similarity Coefficient (DSC) and outperforms all models on end-slice performance, improving patient-specific segmentation accuracy.

Keywords: Ensemble Learning · Uncertainty · Semantic Segmentation

1 Introduction

The cardiac cine technique in cardiac magnetic resonance (CMR) imaging has become the gold standard for the non-invasive assessment of various cardiovascular functions [8]. For ventricular segmentation of the left ventricle (LV), right ventricle (RV), and left ventricle myocardium (MYO) from the background (BG), which is a pixelwise semantic segmentation task, the rise of deep learning has freed cardiologists from labor-intensive manual labeling in recent years.

Unlike typical semantic segmentation tasks, cardiac cine sequences are 4D, with three spatial dimensions (depth, height, width) and time. Each 2D slice (height × width) maintains continuity across spatial and temporal dimensions. Clinically, emphasis is placed on end-diastolic (ED) and end-systolic (ES) phases, so the raw data mainly consists of 3D frames from these phases.

Researchers address this task through two approaches. One treats the entire 3D frame as input and employs a 3D UNet for segmentation (3D-based) [7, 16]. However, several studies pointed out that sequential convolution and pooling operations during the UNet encoder phase inherently struggle to learn long-range relationships between pixels [18, 22], sometimes leading to misidentification of multiple ventricles. The other approach slices the 3D frame into individual 2D

slices [3, 4, 17, 20, 21]. It enhances segmentation accuracy on a single 2D slice by incorporating mechanisms such as Vision Transformer (attention-based), which can achieve strong numerical performance on overall segmentation. However, clinically, differences between 88% and 93% performance are often indistinguishable. Moreover, this approach significantly underperforms on end slices, e.g., the first and last slice of the 3D frame, compared to the middle where ventricular volumes are more pronounced (see Section 4.2). Therefore, there is still a gap in maintaining high segmentation accuracy overall and on the end slices.

In summary, our contributions are as follows:

– **Quantification on End Slices**: We propose a metric in Eq. 7 to evaluate segmentation performance specifically on the end slices for each model and conduct benchmarks on current cutting-edge models.
– **Comprehensive Ensemble Strategies**: We design an end-to-end pipeline Streaming with neural networks as base classifiers, enabling a straightforward integration of outputs from individual classifiers to mitigate the challenges of learning long-range relationships in single classifiers.
– **Memory-based Uncertainty Mechanism**: We compare weight allocation strategies in ensemble learning and introduce a novel approach, termed Memory-based Uncertainty, which leverages global information extracted from 3D frames. Using this approach for weight allocation in our Streaming, we achieve near state-of-the-art (SOTA) performance in overall 3D frame segmentation and significantly improve segmentation accuracy on end slices.

2   Related Works

Ensemble Learning Müller et al. [14] reviewed three ensemble techniques in medical imaging: *Bagging*, *Stacking*, and *Augmenting*, which are contrasted with our framework Streaming in Fig. 1. *Stacking* trains different networks (i.e. heterogeneous) on the same dataset and pools their outputs, while *Bagging* trains the same type of network (i.e. homogeneous) on different trainsets and aggregates predictions on a shared testset. *Augmenting*, in contrast, uses a single network to process augmented test data, combining outputs via pooling. These methods do not fully exploit deep learning's end-to-end nature. Our Streaming unifies the dataset and loss function across all components, streamlining training (see Section.3). Unlike traditional pooling methods that aggregate features such as Voting, our approach uses Weighted Average.

Uncertainty for Segmentation Kendall and Gal [9, 10, 12] proposed the use of Bayesian networks to simultaneously manage aleatoric uncertainties caused by data and epistemic uncertainties caused by the network per se. However, these studies focus primarily on integrating uncertainty into the loss function of an existing single segmentation network to optimize its training process. They do not consider leveraging uncertainty to allocate weights among multiple diverse networks to capitalize on their respective strengths within ensemble learning.
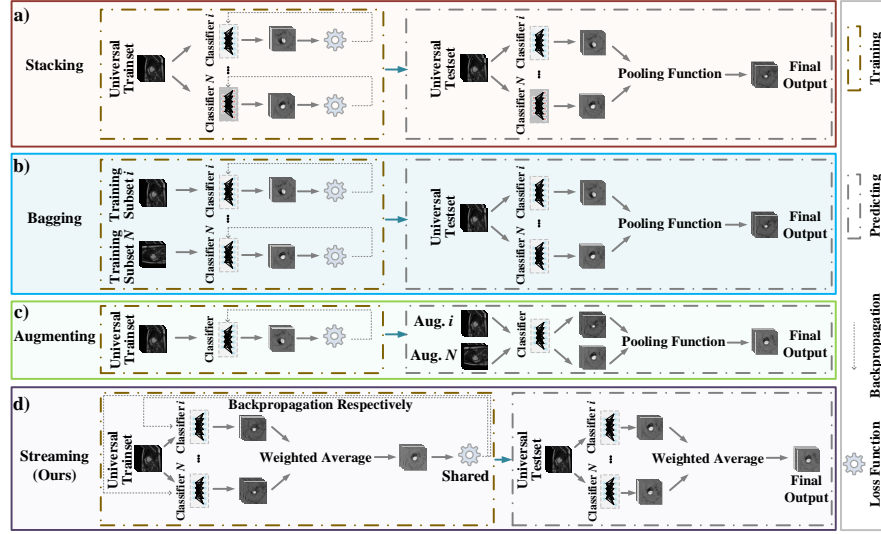
Fig. 1. Visual differences between traditional ensemble learning and ours.

3   Methodology

Ensemble Strategy We define superadditive among classifiers as follows:

$$f(\{\hat{y}_i(\mathbf{x})\}_N) \succeq \frac{1}{N} \sum_{i=1}^{N} \hat{y}_i(\mathbf{x}), \quad \hat{y}_i(\mathbf{x}) \in \mathbb{R}^{+}_{D \times 4 \times H \times W}, \tag{1}$$

where $\mathbf{x}$ is an arbitrary 3D frame from the 4D cardiac cine sequence sample space $\mathcal{X}$. The ensemble method is denoted as $f(\cdot)$, with N classifiers. $\hat{y}_i(\mathbf{x})$ is the probabilities of the i-th classifier's segmentation prediction. The four channels represent BG, RV, MYO, and LV, while D, H, W denote the depth, height, and width of the 3D frame. $\succeq$ indicates that classifiers collaborate better on the Average DSC metric in Eq. 6 than working individually.

To synthesize the outputs from multiple classifiers for superadditive improvement, an intuition is to construct a convex combination, and then use the Softmax function to implement Majority Vote Soft pooling in ensemble learning:

$$\hat{y}(\mathbf{x}) = \text{Softmax}\left(\sum_{i=1}^{N} \omega_i \cdot \hat{y}_i(\mathbf{x})\right) \quad, \quad \text{s.t.} \sum_{i=1}^{N} \omega_i = 1, \quad \omega_i \in \mathbb{R}^{+}, \tag{2}$$

where ω_i is the prior fixed weight (say 0.5) of the i-th classifier. We adopted this approach as a baseline for ablation in our experiments (denoted as *Fixed*).

A more refined method is dynamically allocating weights at the pixelwise level based on the performance of different classifiers. Therefore, we propose:

$$\hat{y}(\mathbf{x}) = \text{Softmax}\left(\sum_{i=1}^{N} \bar{\boldsymbol{\omega}}_i \odot \hat{y}_i(\mathbf{x})\right), \tag{3}$$

$$\text{s.t.} \begin{cases} \boldsymbol{\mu}_i = Mean_D(\hat{y}_i(\mathbf{x})), & \boldsymbol{\mu}_i \in \mathbb{R}^+_{4 \times H \times W} \\[2mm] \boldsymbol{\sigma}_i = Var_{channel}(\boldsymbol{\mu}_i), & \boldsymbol{\sigma}_i \in \mathbb{R}^+_{H \times W} \\[2mm] \bar{\boldsymbol{\omega}}_i = \dfrac{\exp(\boldsymbol{\sigma}_i)}{\sum_{i=1}^{N} \exp(\boldsymbol{\sigma}_i)}, & \sum_{i=1}^{N} \bar{\boldsymbol{\omega}}_i = J_{H \times W} \end{cases}$$

where the mean $\boldsymbol{\mu}_i$ is computed along the depth dimension, representing the likelihood of each channel at each pixel. The uncertainty of the i-th classifier is the variance $\boldsymbol{\sigma}_i$ of $\boldsymbol{\mu}_i$ along the *channel* dimension, where higher variance indicates higher consistency to a channel across multiple slices, thus lower uncertainty (i.e., higher variance between channels indicates the i-th classifier's high confidence in a specific class, allowed to dominate the ensemble). J is an all-ones $H \times W$ matrix, indicating a finer-grained convex combination. $\bar{\boldsymbol{\omega}}_i$, positively correlated with $\boldsymbol{\sigma}_i$, is obtained through exponentiation and regularization, then broadcasted to $D \times 4 \times H \times W$ to perform the Hadamard product $\odot$ with $\hat{y}_i(\mathbf{x})$.

Thus, the forward process uses uncertainty by having the i-th classifier independently predict each 3D frame, storing $\boldsymbol{\sigma}_i$ as memory. During pooling, it dynamically assigns pixelwise weights $\bar{\boldsymbol{\omega}}_i$ based on $\boldsymbol{\sigma}_i$, which leverages spatial continuity to make slices could refer to each other and stabilize performance on end slices. To encourage diverse feature learning, we apply Dropout ($p = 0.5$) at the bottleneck between the encoder and decoder of each classifier.

Loss Function Since RV, MYO, and LV in CMR images exhibit a highly imbalanced distribution, with BG occupying most of the image, our loss function is designed as follows to better handle hard-to-classify samples:

$$\begin{cases} \mathcal{L}_{\text{Dice}}(\hat{y}, y) = \sum_{j=1}^{4} \lambda_j (1 - \text{DSC}(\hat{y}_j, y_j)) \\[4mm] \mathcal{L}_{\text{Focal}}(\hat{y}, y) = -\sum_{j=1}^{4} \alpha_j (1 - \hat{y}_j)^{\gamma} y_j \log \hat{y}_j \\[4mm] \mathcal{L}_{\text{Total}} = \mathcal{L}_{\text{Dice}} + 10 \mathcal{L}_{\text{Focal}} \end{cases} \tag{4}$$

where $\hat{y}_j$ and y_j are the predicted probabilities and ground truth 0-1 mask for each class j. $\mathcal{L}_{\text{Dice}}$ is the weighted Dice loss, with DSC from Eq. 6 and weights $\lambda_j = 2$ for RV, 1 for BG, MYO, and LV. $\mathcal{L}_{\text{Focal}}$ is the Focal Loss [13], with $\alpha_j = 0.1$ and $\gamma = 2$. The total loss $\mathcal{L}_{\text{Total}}$ is a weighted sum of Dice and Focal losses with weights 1 and 10, respectively.

End-to-end Training For the i-th classifier, the gradient for training is:

$$\frac{\partial \mathcal{L}_{\text{Total}}}{\partial \Theta_i} = \frac{\partial \mathcal{L}_{\text{Total}}}{\partial \hat{y}} \cdot \frac{\partial (\text{Softmax}(\sum_{i=1}^{N} \bar{\boldsymbol{\omega}}_i \odot \hat{y}_i))}{\partial \hat{y}_i} \cdot \frac{\partial \hat{y}_i}{\partial \Theta_i}, \tag{5}$$

where Θ_i is the parameters of the i-th classifier, $\bar{\boldsymbol{\omega}}_i$ participates in gradient backpropagation, with each component being fully differentiable to enable efficient gradient flow, allowing Θ_i to be optimized optimized in an end-to-end manner.

4   Experiments

4.1   Setting

Datasets The first dataset we used is ACDC (Automatic Cardiac Diagnosis Challenge) dataset [1], initiated by the MICCAI challenge in 2017, which includes 150 patient cases. The second is M&Ms (The Multi-Centre, Multi-Vendor, and Multi-Disease Cardiac Segmentation) Challenge [2], organized at the MICCAI 2020 STACOM Workshop, consisting of 375 participants from six hospitals. Expert clinicians manually annotated both datasets' LV, RV, and MYO at the ED and ES phases. The trainset and testset have been pre-split by the committee.

Pre-processing and Hyperparameters To process the raw datasets into a suitable format for training, we applied the following steps:

1. **Size correction**. For each patient's slices, we resized the images to 224×224 pixels in height and width using zooming.
2. **Data augmentation**. We applied spatial augmentation, including rotation and flipping, to generate additional training samples.
3. **Normalization**. We kept the category labels unchanged. For each pixel in the original 3D frame, we normalized its grayscale value to the $[0, 1]$.

We chose UNet and DeepLabV3+ (denoted as D3P) without pretraining as our base classifiers to conduct comparison and ablation experiments on an NVIDIA RTX A5000 with 24 GB of GPU memory. Both have a maximum of 256 channels in the bottleneck. The batch size was set to 8, and the number of epochs to 500. All classifiers shared a single optimizer *RMSprop* with a learning rate of 1×10^{-4}, a weight decay of 1×10^{-7}, and a momentum of 0.9. We made our source code publicly available[4].

Metrics To evaluate the quality of segmentation, we employed three metrics:

1. Dice Similarity Coefficient (DSC):

$$DSC(\hat{y}_j, y_j) = \frac{2|\hat{y}_j \cap y_j|}{|\hat{y}_j| + |y_j|}, \tag{6}$$

   where $\hat{y}_j$ and y_j are the predicted probabilities and ground truth 0-1 mask for each class j. It measures the degree of overlapping for class j.
2. End coefficient (EC):

$$EC(\hat{y}_{end}, y_{end}) = \frac{1}{K} \sum_{k=1}^{K} \mathbb{I}(DSC_{Avg}(\hat{y}_{end}, y_{end}) > 0.8) \tag{7}$$

   where $\hat{y}_{end}$ is the segmented mask of the first and last two slices of a 3D frame, and y_{end} is the ground truth. $\mathbb{I}$ is the indicator function, which takes the value 1 if the Average DSC on end slices $DSC_{Avg}(\hat{y}_{end}, y_{end})$ is larger than the threshold 0.8, and 0 otherwise. K is the total number of 3D frames.

---

[4] https://github.com/LEw1sin/Uncertainty-Ensemble

3. Hausdorff distance (HD):

$$HD(\hat{y}_j, y_j) = max\{\sup_{p \in \hat{y}_j} d(p, y_j), \sup_{g \in y_j} d(g, \hat{y}_j)\}, \tag{8}$$

which measures the maximum discrepancy between the volumes. We use this metric in Ablation Studies for a more detailed comparison.

4.2   Results

Comparison on ACDC and M&Ms We conducted comparisons and benchmarks with cutting-edge models on ACDC and M&Ms datasets, with results presented in Tab. 1 and Tab. 2 (n/a indicates the model is unavailable). In Tab. 1, No. 1-2 are 3D-based, while No. 3-7 are attention-based. In Tab. 2, except attention-based No. 2, the rest are fine-tuned variants of UNet. The results demonstrate that our framework achieves near SOTA performance on both ACDC and M&Ms in terms of average DSC for RV, MYO, and LV. Moreover, it outperforms existing works on EC, making it more suitable for clinical segmentation of patient-specific samples (e.g., an EC of 81% means the model has 81% confidence in segmenting end slices).

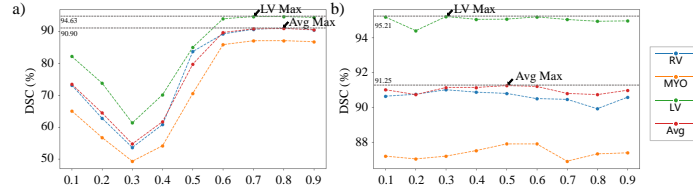**Table 1.** Comparison Study on DSC, and EC Performance on ACDC (↑)

No.	Architectures	Average	RV	MYO	LV	EC
1	2D&3D UNets [7]	91.92	90.78	90.46	94.54	n/a
2	2D-3D FCNN [16]	88.33	87.00	85.50	92.50	n/a
3	TransUNet [4]	89.71	88.96	84.53	95.73	52.83
4	SwinUNet [3]	90.00	88.55	85.62	95.83	48.75
5	SAUNet [20]	91.30	91.40	88.70	93.80	46.98
6	Parallel MERIT [17]	92.32	90.87	90.00	**96.08**	51.32
7	FCT [21]	**93.02**	**92.64**	**90.51**	95.90	48.41
8	**2UNet (Uncertainty, Ours)**	92.29	92.11	89.04	95.73	**81.00**
9	**3UNet (Uncertainty, Ours)**	92.16	91.90	88.99	95.58	69.00

Ablation on ACDC First, we evaluated Streaming with *Fixed* to identify the optimal weights as a baseline for ablation studies. Visual results are in Fig. 2. The homogeneous combination 2UNet with weights (0.5, 0.5) achieves better overall performance, with an average DSC of 91.25. For the heterogeneous combination 1UNet + 1D3P, the highest DSC 90.90 is achieved with weights (0.7, 0.3).

Then, we compared *Stacking, Bagging, Augmenting* the optimal Streaming with *Fixed* (*Stacking, Bagging, Augmenting* also taking Weighted Average as the pooling function, the same weights as *Fixed* for fairness) with our Streaming with Uncertainty, with results in Tab. 3. The observations are as follows:
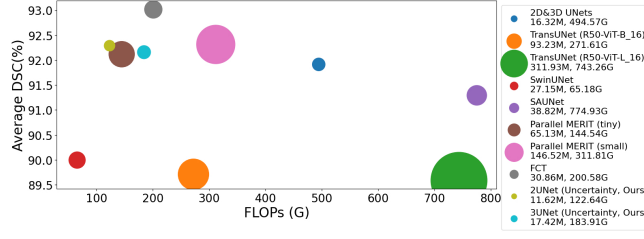
Table 2. Comparison Study on DSC, and EC Performance on M&Ms (↑)

No.	Architectures	Average	RV	MYO	LV	EC
1	UNet [19]	85.70	84.55	82.55	90.00	74.51
2	Attention UNet+CycleGAN [11]	86.57	86.00	83.30	90.40	n/a
3	UNet+DA+DUNN [5]	86.62	86.30	83.35	90.20	76.14
4	UNet (ResNet-34) [15]	87.00	85.75	84.10	91.15	76.75
5	nnUNet [6]	**88.35**	**88.50**	**85.30**	91.25	79.48
6	**2UNet (Uncertainty, Ours)**	87.61	87.70	83.16	91.97	84.93
7	**3UNet (Uncertainty, Ours)**	88.13	88.36	83.78	**92.25**	**88.13**

Fig. 2. a) shows results from 1UNet + 1D3P, with the x-axis varying UNet's weight. b) shows results from 2UNet, with the x-axis varying UNet 1's weight.

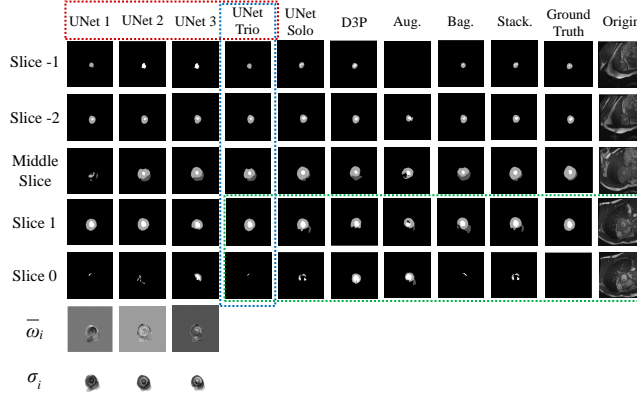**Table 3.** Ablation Study on DSC, HD, and EC Performance on ACDC

Architectures	Average		RV		MYO		LV		EC
	DSC	HD	DSC	HD	DSC	HD	DSC	HD	
UNet	91.27	22.19	90.62	37.29	87.93	18.76	95.28	10.51	53.00
D3P	89.45	27.53	89.41	37.91	85.23	27.22	93.71	17.45	35.00
1UNet + 1D3P (*Fixed*)	90.90	14.00	90.63	17.09	87.47	15.67	94.60	9.22	70.00
1UNet + 1D3P (*Stacking*)	91.38	20.11	90.75	33.81	88.07	17.74	95.32	8.77	54.00
1UNet + 1D3P (Uncertainty)	90.89	13.27	90.41	20.16	87.63	11.34	94.62	8.30	38.00
2UNet (*Fixed*)	91.25	13.32	91.06	18.20	87.59	11.67	95.10	10.09	71.00
2UNet (*Bagging*)	91.71	14.59	90.95	**12.08**	88.66	17.59	95.53	14.10	73.00
2UNet (*Augmenting*)	69.90	27.09	59.36	33.23	69.60	29.27	80.76	18.76	22.00
2UNet (Uncertainty, Ours)	**92.29**	10.33	**92.11**	13.66	**89.04**	10.28	**95.73**	7.06	**81.00**
3UNet (Uncertainty, Ours)	92.16	**10.10**	91.90	16.78	88.99	**8.05**	95.58	**5.46**	69.00
4UNet (Uncertainty)	91.98	12.54	91.80	15.98	88.71	11.29	95.44	10.36	68.00

- **obs 1)** Homogeneous ensembles weighted by Streaming with Uncertainty, together with *Bagging* and *Stacking* are superadditive. 2UNet with Uncertainty is the most stable on DSC and EC, while 3UNet with Uncertainty is the most stable on HD.
- **obs 2)** Our Streaming with Uncertainty outperforms traditional ensemble methods on overall performance. However, increasing the number of classifiers does not consistently improve segmentation performance, and two homogeneous classifiers achieve the best results.

Fig. 3. Test FLOPs and parameters on a 3D frame, marker size shows parameter count.

Computational Efficiency Ensemble learning often faces complexity issues. Compared to baselines on ACDC, ours achieves near-SOTA Average DSC with low parameters and FLOPs, thanks to zero attention, as shown in Fig. 3.

Fig. 4. UNet Trio is 3UNet (Uncertainty), and UNet i is one of its components. Solo means working individually. -1 and -2 are the last two slices, 0 and 1 the first two.

We visualized a challenging sample from the ACDC testset in Fig. 4, the ES frame of patient114 from the hypertrophic cardiomyopathy (HCM) group. The blue box highlights the best-performing model, while the green box shows challenges in other baselines. The last two rows of the first column show $\boldsymbol{\sigma}_i$ and $\bar{\boldsymbol{\omega}}_i$. Uncertainty is mainly concentrated at ventricular and chamber boundaries.

5   Conclusion

In this work, we propose an ensemble paradigm Streaming that retains deep learning's end-to-end benefits. Evaluating on ACDC and M&Ms CMR datasets, together with 3D-based, attention-based models and traditional ensemble strategies, Streaming with Uncertainty achieves near-SOTA performance on DSC and outperforms all models on EC, making it more suitable for clinical applications.

References

1. Bernard, O., Lalande, A., Zotti, C., Cervenansky, F., Yang, X., Heng, P.A., Cetin, I., Lekadir, K., Camara, O., Ballester, M.A.G., et al.: Deep learning techniques for automatic mri cardiac multi-structures segmentation and diagnosis: is the problem solved? IEEE transactions on medical imaging **37**(11), 2514–2525 (2018)
2. Campello, V.M., Gkontra, P., Izquierdo, C., Martin-Isla, C., Sojoudi, A., Full, P.M., Maier-Hein, K., Zhang, Y., He, Z., Ma, J., et al.: Multi-centre, multi-vendor and multi-disease cardiac segmentation: the m&ms challenge. IEEE Transactions on Medical Imaging **40**(12), 3543–3554 (2021)
3. Cao, H., Wang, Y., Chen, J., Jiang, D., Zhang, X., Tian, Q., Wang, M.: Swin-unet: Unet-like pure transformer for medical image segmentation. In: European conference on computer vision. pp. 205–218. Springer (2022)
4. Chen, J., Lu, Y., Yu, Q., Luo, X., Adeli, E., Wang, Y., Lu, L., Yuille, A.L., Zhou, Y.: Transunet: Transformers make strong encoders for medical image segmentation. arXiv preprint arXiv:2102.04306 (2021)
5. Corral Acero, J., Sundaresan, V., Dinsdale, N., Grau, V., Jenkinson, M.: A 2-step deep learning method with domain adaptation for multi-centre, multi-vendor and multi-disease cardiac magnetic resonance segmentation. In: Statistical Atlases and Computational Models of the Heart. M&Ms and EMIDEC Challenges: 11th International Workshop, STACOM 2020, Held in Conjunction with MICCAI 2020, Lima, Peru, October 4, 2020, Revised Selected Papers 11. pp. 196–207. Springer (2021)
6. Full, P.M., Isensee, F., Jäger, P.F., Maier-Hein, K.: Studying robustness of semantic segmentation under domain shift in cardiac mri. In: Statistical Atlases and Computational Models of the Heart. M&Ms and EMIDEC Challenges: 11th International Workshop, STACOM 2020, Held in Conjunction with MICCAI 2020, Lima, Peru, October 4, 2020, Revised Selected Papers 11. pp. 238–249. Springer (2021)
7. Isensee, F., Jaeger, P.F., Full, P.M., Wolf, I., Engelhardt, S., Maier-Hein, K.H.: Automatic cardiac disease assessment on cine-mri via time-series segmentation and domain specific features. In: Statistical Atlases and Computational Models of the Heart. ACDC and MMWHS Challenges: 8th International Workshop, STACOM 2017, Held in Conjunction with MICCAI 2017, Quebec City, Canada, September 10-14, 2017, Revised Selected Papers 8. pp. 120–129. Springer (2018)
8. Ismail, T.F., Hua, A., Plein, S., D'Cruz, D.P., Fernando, M.M., Friedrich, M.G., Zellweger, M.J., Giorgetti, A., Caobelli, F., Haaf, P.: The role of cardiovascular magnetic resonance in the evaluation of acute myocarditis and inflammatory cardiomyopathies in clinical practice—a comprehensive review. European heart journal-cardiovascular imaging **23**(4), 450–464 (2022)
9. Kendall, A., Badrinarayanan, V., Cipolla, R.: Bayesian segnet: Model uncertainty in deep convolutional encoder-decoder architectures for scene understanding. arXiv preprint arXiv:1511.02680 (2015)
10. Kendall, A., Gal, Y.: What uncertainties do we need in bayesian deep learning for computer vision? Advances in neural information processing systems **30** (2017)
11. Kong, F., Shadden, S.C.: A generalizable deep-learning approach for cardiac magnetic resonance image segmentation using image augmentation and attention u-net. In: Statistical Atlases and Computational Models of the Heart. M&Ms and EMIDEC Challenges: 11th International Workshop, STACOM 2020, Held in Conjunction with MICCAI 2020, Lima, Peru, October 4, 2020, Revised Selected Papers 11. pp. 287–296. Springer (2021)

12. Li, Y., Gal, Y.: Dropout inference in bayesian neural networks with alpha-divergences. In: International conference on machine learning. pp. 2052–2061. PMLR (2017)
13. Lin, T.Y., Goyal, P., Girshick, R., He, K., Dollár, P.: Focal loss for dense object detection. In: Proceedings of the IEEE international conference on computer vision. pp. 2980–2988 (2017)
14. Müller, D., Soto-Rey, I., Kramer, F.: An analysis on ensemble learning optimized medical image classification with deep convolutional neural networks. Ieee Access **10**, 66467–66480 (2022)
15. Parreño, M., Paredes, R., Albiol, A.: Deidentifying mri data domain by iterative backpropagation. In: Statistical Atlases and Computational Models of the Heart. M&Ms and EMIDEC Challenges: 11th International Workshop, STACOM 2020, Held in Conjunction with MICCAI 2020, Lima, Peru, October 4, 2020, Revised Selected Papers 11. pp. 277–286. Springer (2021)
16. Patravali, J., Jain, S., Chilamkurthy, S.: 2d-3d fully convolutional neural networks for cardiac mr segmentation. In: Statistical Atlases and Computational Models of the Heart. ACDC and MMWHS Challenges: 8th International Workshop, STACOM 2017, Held in Conjunction with MICCAI 2017, Quebec City, Canada, September 10-14, 2017, Revised Selected Papers 8. pp. 130–139. Springer (2018)
17. Rahman, M.M., Marculescu, R.: Multi-scale hierarchical vision transformer with cascaded attention decoding for medical image segmentation. In: Medical Imaging with Deep Learning. pp. 1526–1544. PMLR (2024)
18. Ruan, J., Xiang, S.: Vm-unet: Vision mamba unet for medical image segmentation. arXiv preprint arXiv:2402.02491 (2024)
19. Saber, M., Abdelrauof, D., Elattar, M.: Multi-center, multi-vendor, and multi-disease cardiac image segmentation using scale-independent multi-gate unet. In: Statistical Atlases and Computational Models of the Heart. M&Ms and EMIDEC Challenges: 11th International Workshop, STACOM 2020, Held in Conjunction with MICCAI 2020, Lima, Peru, October 4, 2020, Revised Selected Papers 11. pp. 259–268. Springer (2021)
20. Sun, J., Darbehani, F., Zaidi, M., Wang, B.: Saunet: Shape attentive u-net for interpretable medical image segmentation. In: Medical Image Computing and Computer Assisted Intervention–MICCAI 2020: 23rd International Conference, Lima, Peru, October 4–8, 2020, Proceedings, Part IV 23. pp. 797–806. Springer (2020)
21. Tragakis, A., Kaul, C., Murray-Smith, R., Husmeier, D.: The fully convolutional transformer for medical image segmentation. In: Proceedings of the IEEE/CVF Winter Conference on Applications of Computer Vision. pp. 3660–3669 (2023)
22. Yan, X., Tang, H., Sun, S., Ma, H., Kong, D., Xie, X.: After-unet: Axial fusion transformer unet for medical image segmentation. In: Proceedings of the IEEE/CVF winter conference on applications of computer vision. pp. 3971–3981 (2022)